Photocarrier dynamics in transition metal dichalcogenide alloy $Mo_{0.5}W_{0.5}S_2$

Jiaqi He,[1,2] **Dawei He,**[1] **Yongsheng Wang,**[1,*] **and Hui Zhao**[2,3]

[1]*Key laboratory of Luminescence and Optical Information, Ministry of education, Institute of Optoelectronic Technology, Beijing Jiaotong University, Beijing 100044, China*
[2]*Department of Physics and Astronomy, the University of Kansas, Lawrence, Kansas 66045, USA*
[3]*huizhao@ku.edu*
[*]*yshwang@bjtu.edu.cn*

Abstract: We report a transient absorption study of photocarrier dynamics in transition metal dichalcogenide alloy, $Mo_{0.5}W_{0.5}S_2$. Photocarriers were injected by a 400-nm pump pulse and detected by a 660-nm probe pulse. We observed a fast energy relaxation process of about 0.7 ps. The photocarrier lifetime is in the range of 50 - 100 ps, which weakly depends on the injected photocarrier density and is a few times shorter than MoS_2 and WS_2, reflecting the relatively lower crystalline quality of the alloy. Saturable absorption was also observed in $Mo_{0.5}W_{0.5}S_2$, with a saturation energy fluence of 32 μJ cm^{-2}. These results provide important parameters on photocarrier properties of transition metal dichalcogenide alloys.

OCIS codes: (320.7150) Ultrafast spectroscopy; (160.4670) Optical materials; (160.6000) Semiconductor materials.

References and links

1. Q. H. Wang, K. Kalantar-Zadeh, A. Kis, J. N. Coleman, and M. S. Strano, "Electronics and optoelectronics of two-dimensional transition metal dichalcogenides," Nat. Nanotechnol. **7**, 699–712 (2012).
2. K. F. Mak, C. Lee, J. Hone, J. Shan, and T. F. Heinz, "Atomically thin MoS_2: A new direct-gap semiconductor," Phys. Rev. Lett. **105**, 136805 (2010).
3. A. Splendiani, L. Sun, Y. Zhang, T. Li, J. Kim, C. Y. Chim, G. Galli, and F. Wang, "Emerging photoluminescence in monolayer MoS_2," Nano Lett. **10**, 1271–1275 (2010).
4. D. Xiao, G. B. Liu, W. Feng, X. Xu, and W. Yao, "Coupled spin and valley physics in monolayers of MoS_2 and other group-VI dichalcogenides," Phys. Rev. Lett. **108**, 196802 (2012).
5. H. Zeng, J. Dai, W. Yao, D. Xiao, and X. Cui, "Valley polarization in MoS_2 monolayers by optical pumping," Nat. Nanotechnol. **7**, 490–493 (2012).
6. K. F. Mak, K. He, J. Shan, and T. F. Heinz, "Control of valley polarization in monolayer MoS_2 by optical helicity," Nat. Nanotechnol. **7**, 494–498 (2012).
7. K. F. Mak, K. He, C. Lee, G. H. Lee, J. Hone, T. F. Heinz, and J. Shan, "Tightly bound trion in monolayer MoS_2," Nat. Mater. **12**, 207–211 (2013).
8. J. S. Ross, S. Wu, H. Yu, N. J. Ghimire, A. M. Jones, G. Aivazian, J. Yan, D. G. Mandrus, D. Xiao, W. Yao, and X. Xu, "Electrical control of neutral and charged excitons in a monolayer semiconductor," Nat. Commun. **4**, 1474 (2013).
9. A. Chernikov, T. C. Berkelbach, H. M. Hill, A. Rigosi, Y. L. Li, O. B. Aslan, D. R. Reichman, M. S. Hybertsen, and T. F. Heinz, "Exciton binding energy and nonhydrogenic Rydberg series in monolayer WS_2," Phys. Rev. Lett. **113**, 076802 (2014).
10. K. He, N. Kumar, L. Zhao, Z. Wang, K. F. Mak, H. Zhao, and J. Shan, "Tightly bound excitons in monolayer WSe_2," Phys. Rev. Lett. **113**, 026803 (2014).
11. H. Zeng, G.-B. Liu, J. Dai, Y. Yan, B. Zhu, R. He, L. Xie, S. Xu, X. Chen, W. Yao, and X. Cui, "Optical signature of symmetry variations and spin-valley coupling in atomically thin tungsten dichalcogenides," Sci. Rep. **3**, 1608 (2013).

#253223 Received 3 Nov 2015; revised 24 Nov 2015; accepted 11 Dec 2015; published 17 Dec 2015

12. N. Kumar, S. Najmaei, Q. Cui, F. Ceballos, P. M. Ajayan, J. Lou, and H. Zhao, "Second harmonic microscopy of monolayer MoS_2," Phys. Rev. B **87**, 161403 (2013).
13. L. M. Malard, T. V. Alencar, A. P. M. Barboza, K. F. Mak, and A. M. de Paula, "Observation of intense second harmonic generation from MoS_2 atomic crystals," Phys. Rev. B **87**, 201401 (2013).
14. Y. Li, Y. Rao, K. F. Mak, Y. You, S. Wang, C. R. Dean, and T. F. Heinz, "Probing symmetry properties of few-layer MoS_2 and h-BN by optical second-harmonic generation," Nano Lett. **13**, 3329–3333 (2013).
15. A. K. Geim and I. V. Grigorieva, "Van der waals heterostructures," Nature **499**, 419–425 (2013).
16. L. Britnell, R. M. Ribeiro, A. Eckmann, R. Jalil, B. D. Belle, A. Mishchenko, Y.-J. Kim, R. V. Gorbachev, T. Georgiou, S. V. Morozov, A. N. Grigorenko, A. K. Geim, C. Casiraghi, A. H. C. Neto, and K. S. Novoselov, "Strong light-matter interactions in heterostructures of atomically thin films," Science **340**, 1311–1314 (2013).
17. L. Britnell, R. V. Gorbachev, R. Jalil, B. D. Belle, F. Schedin, A. Mishchenko, T. Georgiou, M. I. Katsnelson, L. Eaves, S. V. Morozov, N. M. R. Peres, J. Leist, A. K. Geim, K. S. Novoselov, and L. A. Ponomarenko, "Field-effect tunneling transistor based on vertical graphene heterostructures," Science **335**, 947–950 (2012).
18. Y. F. Chen, J. Y. Xi, D. O. Dumcenco, Z. Liu, K. Suenaga, D. Wang, Z. G. Shuai, Y. S. Huang, and L. M. Xie, "Tunable band gap photoluminescence from atomically thin transition-metal dichalcogenide alloys," ACS Nano **7**, 4610 (2013).
19. H. L. Li, X. D. Duan, X. P. Wu, X. J. Zhuang, H. Zhou, Q. L. Zhang, X. L. Zhu, W. Hu, P. Y. Ren, P. F. Guo, L. Ma, X. P. Fan, X. X. Wang, J. Y. Xu, A. L. Pan, and X. F. Duan, "Growth of alloy $MoS_{2x}Se_{2(1-x)}$ nanosheets with fully tunable chemical compositions and optical properties," J. Am. Chem. Soc. **136**, 3756 (2014).
20. J. Mann, Q. Ma, P. M. Odenthal, M. Isarraraz, D. Le, E. Preciado, D. Barroso, K. Yamaguchi, G. V. Palacio, A. Nguyen, T. Tran, M. Wurch, A. Nguyen, V. Klee, S. Bobek, D. Z. Sun, T. F. Heinz, T. S. Rahman, R. Kawakami, and L. Bartels, "2-dimensional transition metal dichalcogenides with tunable direct band gaps: $MoS_{2(1-x)}Se_{2x}$ monolayers," Adv. Mater. **26**, 1399 (2014).
21. Q. Feng, Y. Zhu, J. Hong, M. Zhang, W. Duan, N. Mao, J. Wu, H. Xu, F. Dong, F. Lin, C. Jin, C. Wang, J. Zhang, and L. Xie, "Growth of large-area 2D $MoS_{2(1-x)}Se_{2x}$ semiconductor alloys," Adv. Mater. **26**, 2648 (2014).
22. S. H. Su, Y. T. Hsu, Y. H. Chang, M. H. Chiu, C. L. Hsu, W. T. Hsu, W. H. Chang, J. H. He, and L. J. Li, "Band gap-tunable molybdenum sulfide selenide monolayer alloy," Small **10**, 2589–2594 (2014).
23. W. T. Zhang, X. D. Li, T. T. Jiang, J. L. Q. Song, Y. Lin, L. X. Zhu, and X. L. Xu, "CVD synthesis of $Mo_{1-x}W_xS_2$ and $MoS_{2(1-x)}Se_{2x}$ alloy monolayers aimed at tuning the bandgap of molybdenum disulfide," Nanoscale **7**, 13554–13560 (2015).
24. Q. L. Feng, N. N. Mao, J. X. Wu, H. Xu, C. M. Wang, J. Zhang, and L. M. Xie, "Growth of $MoS_{2(1-x)}Se_{2x}$ (x = 0.41-1.00) monolayer alloys with controlled morphology by physical vapor deposition," ACS Nano **9**, 7450–7455 (2015).
25. H. L. Li, Q. L. Zhang, X. D. Duan, X. P. Wu, X. P. Fan, X. L. Zhu, X. J. Zhuang, W. Hu, H. Zhou, A. L. Pan, and X. F. Duan, "Lateral growth of composition graded atomic layer $MoS_{2(1-x)}Se_{2x}$ nanosheets," J. Am. Chem. Soc. **137**, 5284–5287 (2015).
26. L. Yang, Q. Fu, W. H. Wang, J. Huang, J. L. Huang, J. Y. Zhang, and B. Xiang, "Large-area synthesis of monolayered $MoS_{2(1-x)}Se_{2x}$ with a tunable band gap and its enhanced electrochemical catalytic activity," Nanoscale **7**, 10490–10497 (2015).
27. V. Klee, E. Preciado, D. Barroso, A. E. Nguyen, C. Lee, K. J. Erickson, M. Triplett, B. Davis, I. H. Lu, S. Bobek, J. McKinley, J. P. Martinez, J. Mann, A. A. Talin, L. Bartels, F. Leonard, and U. S. A., "Superlinear composition-dependent photocurrent in CVD-grown monolayer $MoS_{2(1-x)}Se_{2x}$ alloy devices," Nano Lett. **15**, 2612–2619 (2015).
28. Q. Fu, L. Yang, W. H. Wang, A. Han, J. Huang, P. W. Du, Z. Y. Fan, J. Y. Zhang, and B. Xiang, "Synthesis and enhanced electrochemical catalytic performance of monolayer $WS_{2(10x)}Se_{2x}$ with a tunable band gap," Adv. Mater. **27**, 4732–4738 (2015).
29. Y. F. Chen, D. O. Dumcenco, Y. M. Zhu, X. Zhang, N. N. Mao, Q. L. Feng, M. Zhang, J. Zhang, P. H. Tan, Y. S. Huang, and L. M. Xie, "Composition-dependent raman modes of $Mo_{1-x}W_xS_2$ monolayer alloys," Nanoscale **6**, 2833 (2014).
30. A. Kutana, E. S. Penev, and B. I. Yakobson, "Engineering electronic properties of layered transition-metal dichalcogenide compounds through alloying," Nanoscale **6**, 5820 (2014).
31. S. J. Zheng, L. F. Sun, T. T. Yin, A. M. Dubrovkin, F. C. Liu, Z. Liu, Z. X. Shen, and H. J. Fan, "Monolayers of $W_xMo_{1-x}S_2$ alloy heterostructure with in-plane composition variations," Appl. Phys. Lett. **106**, 063113 (2015).
32. H. F. Liu, K. K. A. Antwi, S. Chua, and D. Z. Chi, "Vapor-phase growth and characterization of $Mo_{1-x}W_xS_2$ atomic layers on 2-inch sapphire substrates," Nanoscale **6**, 624 (2014).
33. J. G. Song, G. H. Ryu, S. J. Lee, S. Sim, C. W. Lee, T. Choi, H. Jung, Y. Kim, Z. Lee, J. M. Myoung, C. Dussarrat, C. Lansalot-Matras, J. Park, H. Choi, and H. Kim, "Controllable synthesis of molybdenum tungsten disulfide alloy for vertically composition-controlled multilayer," Nat. Commun. **6**, 7817 (2015).
34. B. Huang, M. Yoon, B. G. Sumpter, S. H. Wei, and F. Liu, "Alloy engineering of defect properties in semiconductors: Suppression of deep levels in transition-metal dichalcogenides," Phys. Rev. Lett. **115**, 126806 (2015).
35. D. O. Dumcenco, H. Kobayashi, Z. Liu, Y. S. Huang, and K. Suenaga, "Visualization and quantification of transition metal atomic mixing in $Mo_{1-x}W_xS_2$ single layers," Nat. Commun. **4**, 1351 (2013).

#253223 Received 3 Nov 2015; revised 24 Nov 2015; accepted 11 Dec 2015; published 17 Dec 2015

36. S. Yoshida, Y. Kobayashi, R. Sakurada, S. Mori, Y. Miyata, H. Mogi, T. Koyama, O. Takeuchi, and H. Shigekawa, "Microscopic basis for the band engineering of $Mo_{1-x}W_xS_2$-based heterojunction," Sci. Rep. **5**, 14808 (2015).
37. M. Zhang, J. Wu, Y. Zhu, D. O. Dumcenco, J. Hong, N. Mao, S. Deng, Y. Chen, Y. Yang, C. Jin, S. H. Chaki, Y. S. Huang, J. Zhang, and L. Xie, "Two-dimensional molybdenum tungsten diselenide alloys: Photoluminescence, raman scattering, and electrical transport," ACS Nano **8**, 7130–7137 (2014).
38. K. K. Kam and B. A. Parkinson, "Detailed photocurrent spectroscopy of the semiconducting group-vi transition-metal dichalcogenides," J. Phys. Chem. **86**, 463 (1982).
39. A. R. Beal, W. Y. Liang, and H. P. Hughes, "Kramers-Kronig analysis of reflectivity spectra of 3R-WS_2 and 2H-WSe_2," J. Phys. C **9**, 2449 (1976).
40. B. A. Ruzicka, N. Kumar, S. Wang, K. P. Loh, and H. Zhao, "Two-probe study of hot carriers in reduced graphene oxide," J. Appl. Phys. **109**, 084322 (2011).
41. S. Schmitt-Rink, D. S. Chemla, and D. A. B. Miller, "Theory of transient excitonic optical nonlinearities in semiconductor quantum-well structures," Phys. Rev. B **32**, 6601–6609 (1985).
42. J. He, D. He, Y. Wang, Q. Cui, F. Ceballos, and H. Zhao, "Spatiotemporal dynamics of excitons in monolayer and bulk ws_2," Nanoscale **7**, 9526 (2015).
43. N. Kumar, J. He, D. He, Y. Wang, and H. Zhao, "Charge carrier dynamics in bulk MoS_2 crystal studied by transient absorption microscopy," J. of Appl. Phys. **113**, 133702 (2013).
44. H.-P. Komsa and A. V. Krasheninnikov, "Effects of confinement and environment on the electronic structure and exciton binding energy of MoS_2 from first principles," Phys. Rev. B **86**, 241201 (2012).
45. N. Kumar, Q. Cui, F. Ceballos, D. He, Y. Wang, and H. Zhao, "Exciton-exciton annihilation in $MoSe_2$ monolayers," Phys. Rev. B **89**, 125427 (2014).
46. D. Sun, Y. Rao, G. A. Reider, G. Chen, Y. You, L. Brezin, A. R. Harutyunyan, and T. F. Heinz, "Observation of rapid exciton-exciton annihilation in monolayer molybdenum disulfide," Nano Lett. **14**, 5625–5629 (2014).

1. Introduction

Since 2010, transient metal dichalcogenides (TMDs), such as MoS_2 and WS_2 have attracted significant interests as their layered crystal structure allows fabrication of monolayers through simple but effective approaches such as mechanical exfoliation [1]. Although the bandgaps of these bulk TMDs are indirect and are in the near infrared range, their monolayers have direct bandgaps with lowest excitonic states in the visible range [2, 3]. Furthermore, these monolayers have shown other exotic properties, such as valley-selective optical coupling [4–6], large binding energies of excitons, trions, and biexcitons [7–10], and strong nonlinear optical responses [11–14]. In addition, these two-dimensional materials can be used to fabricate new van der Waals heterostructures [15–17].

So far, the most extensively studied TMD members are MoS_2, WS_2, $MoSe_2$, and WSe_2. They have qualitatively similar but quantitatively different electronic structures [1]. Hence, one natural way to expand the horizon of these materials is to fabricate their alloys. In 2013, monolayers of $MoS_{2(1-x)}Se_{2x}$ were first produced by mechanical exfoliation [18]. Tuning of the bandgap by varying the composition was demonstrated by photoluminescence spectroscopy [18]. Chemical vapor deposition (CVD) of monolayer $MoS_{2(1-x)}Se_{2x}$ was soon reported by several groups [19–27]. Similarly, CVD of monolayer $WS_{2(1-x)}Se_{2x}$ with tunable bandgaps was achieved, too [28]. Alloying the transition metal atoms offers another approach to tune the electronic properties. Indeed, monolayers of $Mo_{1-x}W_xS_2$ have been produced by mechanical exfoliation [29], CVD [23, 30, 31], and sulfurization of oxide films [32, 33]. Monolayers of $Mo_{1-x}W_xSe_2$ have also been produced by CVD [34].

The fast progress in developing and optimizing fabrication techniques allows further studies on the properties of TMD alloys. For example, lattice structure and distribution of Mo and W atoms in $Mo_{1-x}W_xS_2$ monolayers were investigated by scanning transmission electron microscopy [35]. Effects of alloy engineering on controlling the detects were studied in $Mo_{1-x}W_xSe_2$ [34]. The electronic structure of monolayer $Mo_{1-x}W_xS_2$ was revealed by scanning tunneling microscopy and spectroscopy [36]. In contrast, optical studies of TMD alloys are rare and are limited to steady state measurements, such as photoluminescence [37], Raman spectroscopy [37], and photocurrent generation [27].

#253223 Received 3 Nov 2015; revised 24 Nov 2015; accepted 11 Dec 2015; published 17 Dec 2015

Here we report the first time-resolved study of carrier dynamics in TMD alloys by using femtosecond transient absorption technique. As an example, we investigated $Mo_{1-x}W_xS_2$ bulk crystals with x = 0.5. We deduced the lifetime of photocarriers and energy relaxation time of hot carriers. The photocarrier dynamics in $Mo_{1-x}W_xS_2$ is also compared with MoS_2 and WS_2. These measurements provide important parameters to understand performance of these TMD alloys in various applications in optoelectronic devices.

2. Experimental section

2.1. Sample preparation

We studied bulk alloy of $Mo_{0.5}W_{0.5}S_2$ provided by 2D Semiconductors. To ensure that the measurements were performed on a single-crystal domain, a mechanical exfoliation procedure was used to obtain films of $Mo_{0.5}W_{0.5}S_2$, which were transferred to a silicon substrate with an oxide layer. The films studied have thicknesses on the order of 100 nm, and can be treated as bulk materials. All the measurements were performed with the sample at room temperature.

2.2. Transient absorption

The dynamics of the photocarriers in $Mo_{0.5}W_{0.5}S_2$ was studied by transient absorption in the reflection geometry. As shown schemitically in Fig. 1, the setup is based on an 80 MHz Ti:sapphire laser that generates 100 fs pulses with a central wavelength of 800 nm. A portion of this beam is focused to a beta barium borate (BBO) crystal to generate its second harmonic at 400 nm. This beam is focused to the sample by a microscope objective lens. This pump pulse injects photocarriers to the sample by interband absorption. The other portion of the 800 nm beam is coupled to a highly chirped photonic crystal fiber (PCF) to generate a supercontinuum radiation in the visible and near infrared range. A dielectric bandpass filter with a central passing wavelength of 660 nm and a bandwidth of 10 nm is used to select that wavelength component from the supercontinuum. This probe beam is combined with the pump beam and focused to the sample through the same objective lens. The focused spot size is about 2.4 μm for both pump and probe beams, which is determined by an imaging system with a precision of about 0.2 μm. The reflected probe is sent to a silicon photodiode, which output is measured by a lock-in amplifier. A long-pass filter prevents the reflected pump beam from reaching the photodiode. A mechanical chopper modulates the pump intensity at about 2 KHz, in order to improve the signal-to-noise ratio. The pump and the probe pulses are orthogonally linearly polarized.

With this configuration, we measure the differential reflection of the probe, $\Delta R/R_0 = (R - R_0)/R_0$, where R and R_0 are the reflection of the probe with and without the presence of the pump beam, respectively. The differential reflection is measured as a function of the probe delay, which is defined as the arrival time of the probe pulse at the sample with respect to the pump pulse. This quantity is controlled by a using a linear stage, which moves a reflector along a line, in the pump arm to vary the pump beam path length.

3. Results and discussion

The electronic bandstructure of $Mo_{1-x}W_xS_2$ alloys has not been precisely determined yet. However, since the bandgaps of MoS_2 and WS_2 bulk crystals are 1.2 and 1.4 eV, respectively [38], the bandgap of $Mo_{0.5}W_{0.5}S_2$ is expected to be in the range of 1.2 - 1.4 eV, and be close to 1.3 eV. In our experiment, the 400-nm pump pulse with a photon energy of 3.1 eV injects photocarriers with an excess energy of about 1.8 eV, which is distributed between the electrons and the holes. These hot carriers injected are expected to relax their energy rapidly to the lattice, moving to the low-energy states in the conduction and valance bands. This energy relaxation

#253223 Received 3 Nov 2015; revised 24 Nov 2015; accepted 11 Dec 2015; published 17 Dec 2015

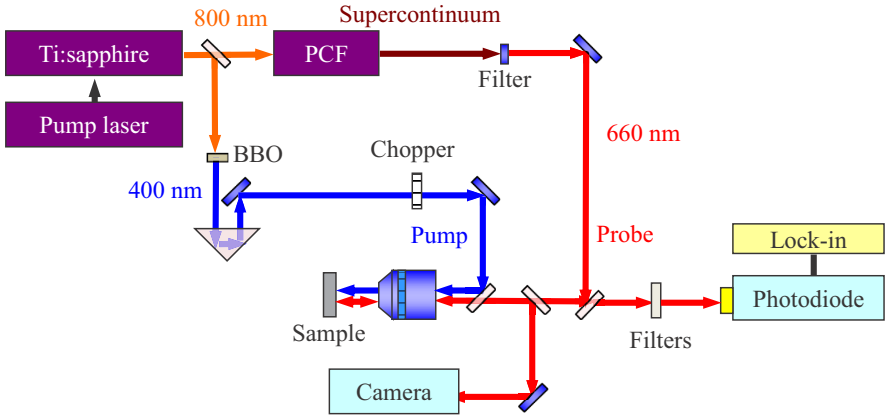

Fig. 1. Transient absorption setup.

process will be followed by a slower recombination process of the photocarriers, determined by their lifetime.

The dynamics of these injected photocarriers are monitored by the 660-nm probe pulse with a photon energy of about 1.9 eV. Hence, it directly probes states in the conduction and valance bands that are about 0.3 eV above the band edges. The observed differential reflection signal is shown in Fig. 2 for short (left) and long (right) time ranges. Different symbols represent measurements with different values of pump fluence, as labeled in the figure. So far, the absorption coefficient of TMD alloys has not been precisely measured, preventing us from accurately determining the injected photocarrier density from the pump fluence. If we assume that the absorption coefficient of $Mo_{0.5}W_{0.5}S_2$ at 400 nm is close to WS_2, which is about 7×10^7 m^{-1} [39], we can roughly estimate that a pump fluence of 1 μJ cm^{-2} corresponds to a photocarrier density of 1.5×10^{18} cm^{-3} at the sample surface.

As shown in the left panel of Fig. 2, the differential reflection signal reaches to a peak rapidly in a few picoseconds. This process can be attributed to the relaxation of photocarriers from the initially injected high energy states to the states probed. We model the rising part of the signal as $N_0(1-e^{-t/\tau_X})$, where N_0 is the peak signal and τ_X describes the associated energy relaxation time [40]. By fitting the signals with probe delays from 0 to 2 ps, we find this simple model is consistent with the data, as indicated by the solid red curves. From these fits, we obtained the relaxation times and the peak values, as summarized in Figs. 3(a) and 3(b). No dependence of the relaxation time on the pump fluence is observed. This is expected, since the energy relaxation of carriers is achieved by phonon emission, which does not strongly depend on the injected carrier density. We obtain an average values of $\tau_X = 0.68 \pm 0.10$ ps. We also find that the peak signal increases with the pump fluence linearly when the fluence is low, and saturates at higher fluences, as shown in Fig. 3(b). This dependence can be satisfactorily described by the saturation model [41], $\Delta R/R_0 \propto F/(F+F_s)$, where F is the pump fluence and F_s the saturation fluence. From a fit, indicated as the red line, we obtain $F_s = 32 \pm 3$ μJ cm^{-2}, which corresponds to a saturation density of about 5×10^{19} cm^{-3}. This quantity describes the effectiveness of photocarriers in saturating the absorption coefficient, and is important for applications as saturable absorbers. Similar saturation effects have been observed in TMDs, too [42, 43].

The right panel of Fig. 2 shows the differential reflection signal on a long time scale. The decay of the signal is caused by loss of photocarrier population due to their recombination. Since

#253223 Received 3 Nov 2015; revised 24 Nov 2015; accepted 11 Dec 2015; published 17 Dec 2015

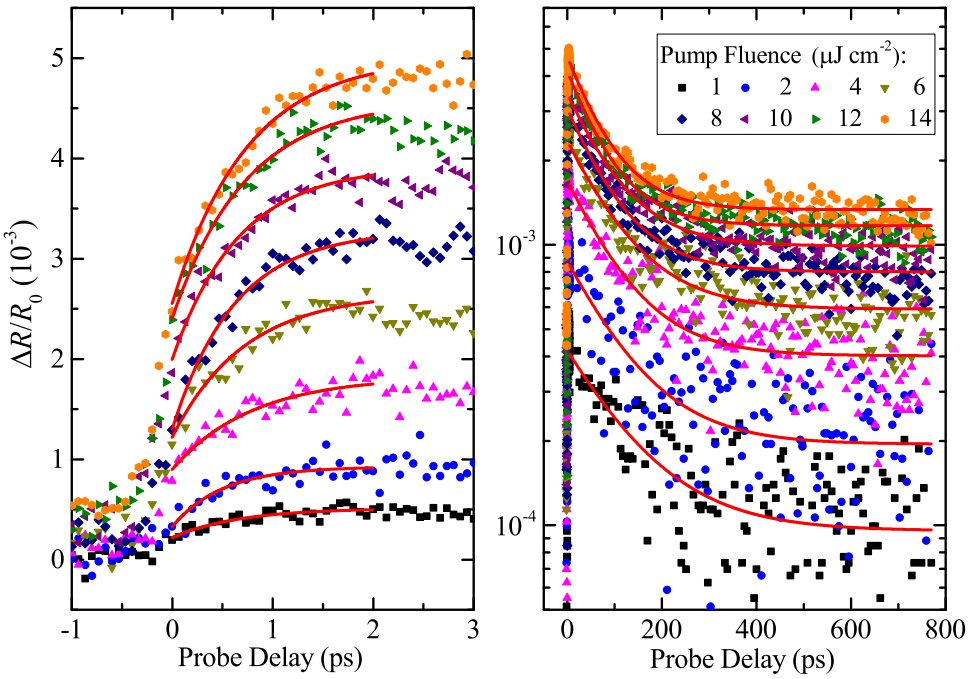

Fig. 2. Differential reflection signal over short (left panel) and long (right panel) time scales, with different values of the pump fluence as labeled. The solid red lines are fits to the data.

the exciton binding energies in TMD bulk crystals are much higher than the room temperature thermal energy [44], the photocarriers are expected to be mostly excitons during this process. We fit the data with a single exponential function, $N_0 e^{-t/\tau_R} + N_R$, as shown as the solid red curves. Clearly, the decay can be satisfactorily described by the single exponential function. The deduced photocarrier lifetime, τ_R, is plotted as a function of the pump fluence in Fig. 3(c). We found that the lifetime decreases with the fluence: it changes from about 100 ps at relatively low fluence to about 50 ps at the highest fluence used in this study. Such an enhanced recombination at high injected carrier densities can be attributed to multi-carrier processes, such as exciton-exciton annihilation, that have been observed in transient metal dichalcogenides [45, 46].

As shown in the right panel of Fig. 2, there is a significant residual of the signal after this single exponential decay process. The magnitude of this residual is proportional to the pump fluence, as shown in Fig. 3(d). This indicates that there is a slower process induced by the pump pulse. Since no signal is observed at negative probe delays, this residual decays on a time scale shorter than 13 ns, which is the separation of two sequential pump pulses in the measurement. It is unlikely that this residual is caused by trapped carriers at defect sites, since it shows no saturation at rather high carrier densities. We attribute this residual to thermal effect left by the carriers, which causes the excited region of the sample to reach a higher lattice temperature.

Finally, we compare the photocarrier dynamics in $Mo_{0.5}W_{0.5}S_2$ with those in MoS_2 and WS_2 bulk crystals. Samples of MoS_2 and WS_2 films were prepared from bulk crystals with a similar procedure as $Mo_{0.5}W_{0.5}S_2$. For each sample, we injected photocarriers with a pump pulse of 400 nm wavelength and 4-μJ cm^{-2} fluence, and used the same 660-nm pulse as the probe. The results are shown in Fig. 4 for short (left) and long (right) time scales. Under the same conditions, the signals from WS_2 and $Mo_{0.5}W_{0.5}S_2$ have similar magnitudes, while MoS_2

#253223 Received 3 Nov 2015; revised 24 Nov 2015; accepted 11 Dec 2015; published 17 Dec 2015

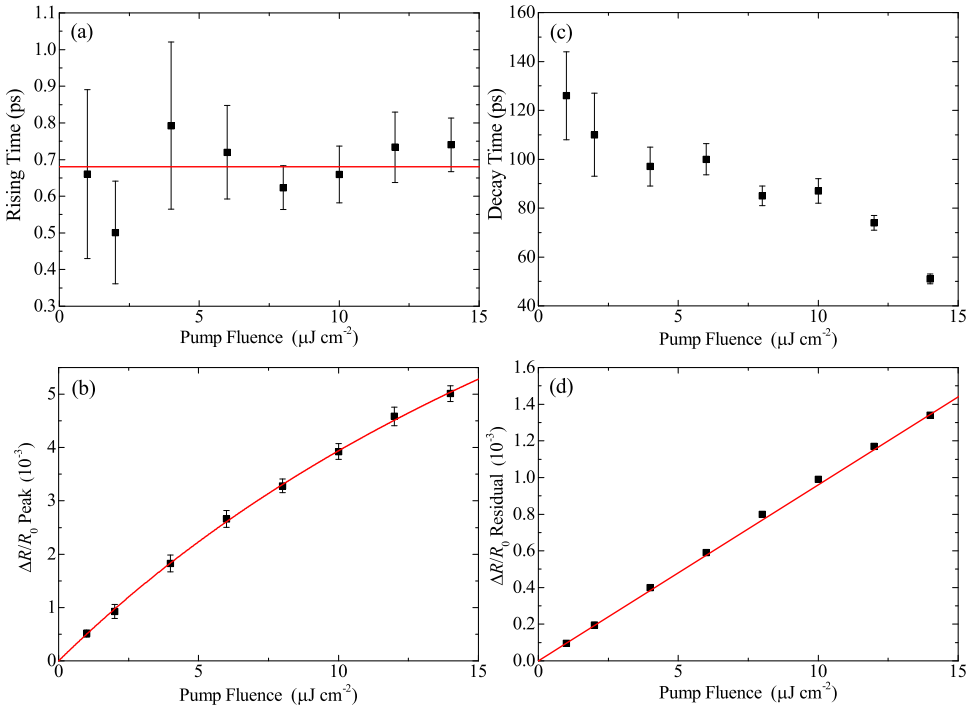

Fig. 3. (a) The rising times of the differential reflection signal deduced from fits shown in Fig. 2 (left panel). The red line indicates an average value of 0.68 ps. (b) The peak value of differential reflection. The red line shows a fit to the data, corresponding to a saturation fluence of 32 μJ cm^{-2}. (c) Decay times of the differential reflection signal. (d) The values of the residual differential reflection signal at long probe delays.

produced a signal of a few times larger. Both MoS_2 and WS_2 have a small peak right after zero delay, which is absent in $Mo_{0.5}W_{0.5}S_2$.

We are mostly interested in comparing the recombination of photocarriers in the three materials. As shown in the right panel of Fig. 4, the decay of the signal in MoS_2 and WS_2 is noticeably slower than $Mo_{0.5}W_{0.5}S_2$. By fitting all the three curves with single exponential functions (red curves), we obtained photocarrier lifetimes of 360 $\pm$ 10 and 240 $\pm$ 20 ps in MoS_2 and WS_2, respectively, both are much longer than the 100 ps obtained in $Mo_{0.5}W_{0.5}S_2$ alloy. The shorter lifetime in $Mo_{0.5}W_{0.5}S_2$ can be attributed to its alloy nature, which results in lower crystalline quality of the lattice. This result also suggests that the recombination lifetime of photocarriers in all these materials are dominated by nonradiative recombination, and reflects the quality of the samples. The radiative recombination time of these indirect semiconductors are expected to be much longer.

4. Conclusion

In summary, we have time resolved photocarrier dynamics in TMD alloys. Differential reflection signals were observed in a $Mo_{0.5}W_{0.5}S_2$ bulk crystal, following interband absorption of an ultrafast pump pulse. An energy relaxation process shorter than 1 ps was observed. The photocarrier lifetime was found to be in the range of 50 - 100 ps, depending on the injected photocarrier density. This is a few times shorter than MoS_2 and WS_2, reflecting the relatively

#253223 Received 3 Nov 2015; revised 24 Nov 2015; accepted 11 Dec 2015; published 17 Dec 2015

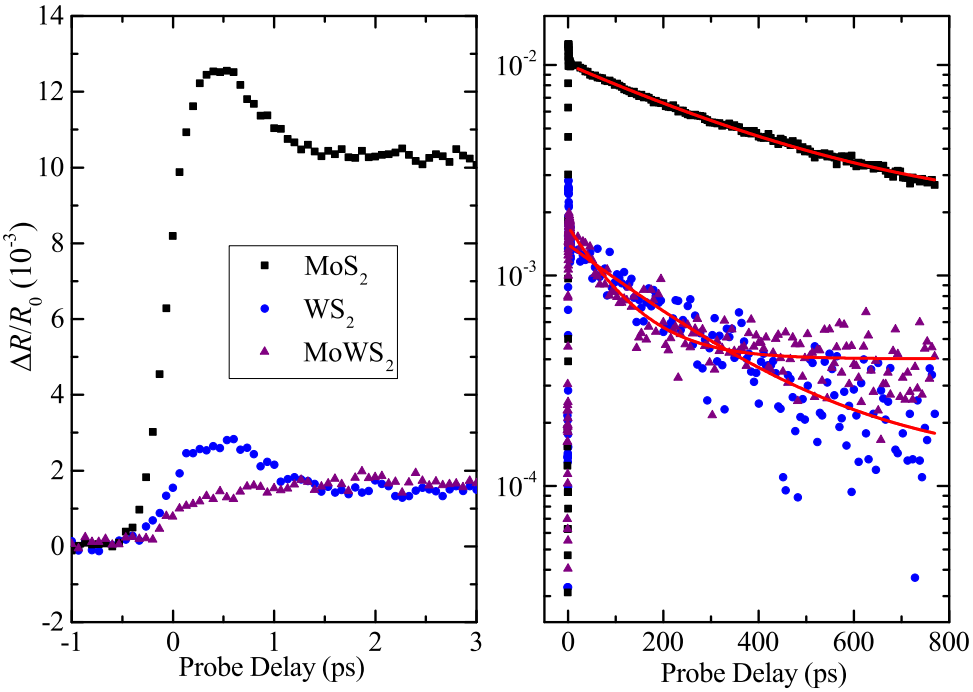

Fig. 4. Differential reflection signal over short (left panel) and long (right panel) time scales measured from MoS_2 (black squares), WS_2 (blue circles), and $Mo_{0.5}W_{0.5}S_2$ (purple triangles). The red lines are single exponential fits.

lower crystalline quality in the alloy. Saturable absorption of TMD alloys was also observed, with a saturation fluence of 32 μJ cm^{-2}. This effect can be utilized in nonlinear photonic and optoelectronic devices. These results provide important parameters on photocarrier properties in TMD alloys.

Acknowledgment

This material is based upon work supported by the National Science Foundation of USA (DMR-1505852, IIA-1430493), Chinese Natural Science Fund Project (61527817, 61335006, 61378073), Beijing Science and Technology Committee (Z151100003315006) and Fundamental Research Funds for the Central Universities (2015YJS181).

#253223 Received 3 Nov 2015; revised 24 Nov 2015; accepted 11 Dec 2015; published 17 Dec 2015